NASA TECHNICAL NOTE

NASA TN D-5293

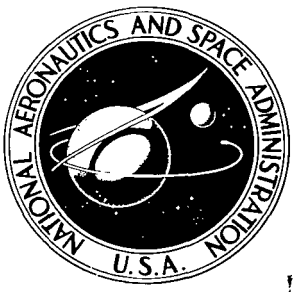

NASA TN D-5293

INTERPLANETARY PROBE MISSIONS WITH SOLAR-ELECTRIC PROPULSION SYSTEMS

by Charles L. Zola

Lewis Research Center
Cleveland, Ohio

NATIONAL AERONAUTICS AND SPACE ADMINISTRATION • WASHINGTON, D. C. • JULY 1969

INTERPLANETARY PROBE MISSIONS WITH SOLAR-ELECTRIC PROPULSION SYSTEMS

By Charles L. Zola

Lewis Research Center
Cleveland, Ohio

NATIONAL AERONAUTICS AND SPACE ADMINISTRATION

For sale by the Clearinghouse for Federal Scientific and Technical Information
Springfield, Virginia 22151 – CFSTI price $3.00

ABSTRACT

A preliminary study is made of trajectories and propulsion system design parameters for solar-electric-propulsion spacecraft for several interplanetary missions. Using the Atlas-Centaur as a common launch vehicle, payload capability comparisons are also made for each mission between the solar-electric propulsion system and an alternative high-performance chemical propulsion upper stage. Payload capability of the solar-electric system is at least 300 kilograms for flyby missions to Jupiter, Saturn, Uranus, and Neptune, with trip times competitive with or shorter than those of ballistic systems. Loose elliptic capture missions to these four planets, as well as Mars and Mercury, can be accomplished with at least 200 kilograms of payload.

INTERPLANETARY PROBE MISSIONS WITH SOLAR-ELECTRIC PROPULSION SYSTEMS

by Charles L. Zola

Lewis Research Center

SUMMARY

A preliminary study is made to identify the best trajectories and propulsion system design parameters for solar-electric-propulsion spacecraft for several interplanetary missions. Also, payload capability comparisons are made between the electric propulsion system and a high-performance all-chemical propulsion system for each mission. System comparisons concerning relative development costs, availability, and reliability are not considered in this report. All systems analyzed are assumed to be launched by the same launch vehicle, Atlas-Centaur. Flyby and loose elliptic capture missions are analyzed and compared for several target planets.

With the launch vehicle and component performances assumed for this study, solar-electric-propulsion flyby missions with at least 300 kilograms of payload are possible for Jupiter, Saturn, Uranus, and Neptune. For the same four planets, the electric propulsion capture missions can place at least 200 kilograms of payload in elliptic parking orbit. Payload capability of the solar-electric system for Mars and Mercury capture missions exceeds 700 and 300 kilograms, respectively. Comparison calculations show that the all-chemical system has a better payload capability than the solar-electric system for Mars and Jupiter missions. The two systems have about equal payload capability for Saturn missions for the particular set of assumptions used in this report. In most cases solar-electric-propulsion trip times are competitive with, or shorter than, those of all-chemical systems. For Uranus and Neptune missions, the solar-electric system can deliver more payload at shorter trip times than the all-chemical system. The major components of the solar-electric propulsion system have a greater potential for future performance improvements than chemical propulsion systems.

INTRODUCTION

Continuing progress in the development of both solar-cell power systems and ion thrusters could lead to useful mission applications of electric propulsion in interplanetary spacecraft. For continuous sunlight operation, current solar-cell systems have proven to be the most lightweight and reliable and the longest duration space power source available. Reference 1 presents an example of design studies that have been made for future large-area, lightweight, solar-cell panel arrays with power output above 10 kilowatts. Reference 2 discusses further improvements that are anticipated in the weight, efficiency, and durability of solar cells. Studies such as reference 3 are producing designs of the necessary power regulation systems that have high efficiency, low weight, and long operating life. Ion thrusters, especially the electron bombardment mercury and cesium types, are steadily increasing in efficiency and operating life (refs. 4 and 5).

This report presents a preliminary analysis of interplanetary probe missions to evaluate the payload capability of the solar-electric-propulsion spacecraft. The solar-cell powerplant and ion thrusters used in this study have been given weight and performance values representative of current technology. It should, however, be noted that solar-electric propulsion systems of the required size, lifetime, and reliability assumed in this study have not yet been built and demonstrated in a flight environment.

A wide range of interplanetary missions are analyzed to more clearly define the areas of applicability of such spacecraft. Reference 6 is a recent similar study which also contains a detailed design study of the important components of the solar-electric propulsion system. This present report does not go into system details but does cover a wider variety of mission targets and trajectory types. In earlier publications, Strack (refs. 7 and 8) made a similar analysis of close-in solar probe missions. In this report, missions to Mercury, Mars, Jupiter, Saturn, Uranus, and Neptune are analyzed. Mission trajectories which include a gravity assist, or swingby, at an intermediate planet are not considered in this study.

Each solar-electric-propulsion mission result is compared with a high-performance all-chemical-propulsion method of carrying out the same mission. For purposes of comparison, both electric and all-chemical probe systems presented in this report are based on a launch from Earth's surface by the same launch vehicle. In this case, a current version of the Atlas-Centaur launch vehicle is used.

This report must be considered preliminary because many simplifying assumptions in mission trajectory calculations and spacecraft subsystems performance have been made to allow a broad scope of coverage in mission targets and mission modes. Therefore, the payload values presented are optimistic and represent the probable upper limits of performance for both the all-chemical and solar-electric propulsion systems

assumed for the present study. Probe missions to Mercury, Mars, Jupiter, Saturn, Uranus, and Neptune are analyzed. Weight and performance assumptions for the solar-electric and chemical propulsion subsystems are presented in detail in the ANALYSIS section. Examples of solar-electric-propulsion spacecraft weight summaries and optimum design parameters are given in appendix B. (Symbols are defined in appendix A, and performance calculations for the hypothetical kick stage are given in appendix C.)

ANALYSIS

Mission Profiles

The interplanetary missions analyzed in this report are divided into two basic mission modes, flybys and captures. Each of the two modes are further subdivided into those profiles using only high-thrust chemical propulsion or those which also use low-thrust solar-electric propulsion.

The objective of the flyby mode is to allow the spacecraft one close encounter with the target planet. The flyby mode allows the delivery of the most payload to each planet since its trajectory requires less propulsive effort than any other that may be used for the same transfer time. The capture mission, however, aims to place the probe payload in a parking orbit about the target planet. The use of a final parking orbit allows repeated close encounters with the planet surface to gather more scientific data over a longer time, thereby overcoming the major disadvantage of flyby missions. For a given target planet, the payload of a capture mission is always less than that of a flyby mission of the same transfer time. The lower payload is due to the extra propulsive maneuvers required in capture missions. The highest payload capture mission has an elliptic parking orbit at the target planet with a low periapsis and very high apoapsis. For either the all-chemical or solar-electric-propulsion cases, the analysis assumes that a small storable chemical braking rocket system is carried on all capture missions. The braking system is used to bring the velocity of the spacecraft to just below the escape value at periapsis. The best periapsis for each planet would depend on the scientific objectives of the probe mission. However, for consistency in this study, the periapsis of all capture missions is fixed at 2 planet radii.

The launch system used in the all-chemical missions for this report is an Atlas-Centaur with an additional high-energy chemical propulsion upper stage (kick stage) to improve the high-velocity injection payload at Earth. The Atlas - Centaur - kick stage combination is used only in the all-chemical missions. These missions are referred to as ACK flyby or capture missions in the remainder of this report.

Two different types of solar-electric-propulsion mission profiles are analyzed in this study for both flyby and capture missions. These profiles differ only in the method

of Earth departure. One case is called the spiral-electric, or SE, mission profile. The SE profile uses a low-thrust electric propulsion spiral path to escape Earth from a low circular orbit. The escape spiral is followed by a low-thrust heliocentric transfer. The second type of electric propulsion profile uses the Atlas-Centaur booster to launch the electric spacecraft to escape velocity or higher at the start of the mission. This high-velocity departure is also followed by a low-thrust electric propulsion heliocentric transfer. Since in this second case the electric spacecraft always starts the mission with some amount of hyperbolic excess velocity, this profile is called the hyperbolic-electric, or HE, mission profile.

Mission Trajectories

For the purpose of this preliminary study, a simplified two-dimensional solar system model is assumed with the planets in circular orbit at their mean distances from the Sun. Each interplanetary path is calculated as a sequence of two-body trajectory segments. The planet-centered and Sun-centered two-body trajectories are assumed to patch, or join, at some large distance from each planet. The radius of this patching distance is called the sphere of influence of the planet. A set of numerical constants used for each of the planets in this study is given in table I.

The trajectories used in this report for ACK, HE, or SE missions are straightforward flights from Earth to the target planet, as opposed to trajectories with a gravity assist or swingby at an intermediate planet. A swingby trajectory option can benefit either high-thrust ballistic or solar-electric propulsion missions by shortening trip times and increasing payload. Although swingby options are not included in the scope of this report, it should be noted that their advantages can be offset by limitations on launch opportunity. For example, Saturn missions by means of a Jupiter swingby follow a 20-year cycle. Missions to other outer planets by means of the Jupiter swingby follow a 12-year cycle. The best swingby benefit to these missions in time or payload is only available during about 25 percent of these cycles. On the other hand, launch opportunities for missions without swingby trajectories to the planets beyond Jupiter repeat on a 1-year cycle.

All missions studied in this report, ACK, SE, or HE profiles, essentially start at Earth's surface. In the ACK mission, see sketch (a), the Atlas - Centaur - kick stage launch vehicle leaves the surface and, at 185 kilometers (100 n mi) altitude, injects the spacecraft into a departure trajectory. The injection velocity V_b is high above circular orbit speed V_c, often by as much as 7000 meters per second. The spacecraft coasts to the sphere of influence on a high-energy hyperbolic departure path. At the sphere of influence, the velocity of the spacecraft relative to Earth V_s is vectorially added to Earth's heliocentric orbit velocity V_E. With the proper orientation and magnitude of V_s, the re-

TABLE I. - ASSUMED PLANET CONSTANTS

Constant	Sun	Mercury	Earth	Mars	Jupiter	Saturn	Uranus	Neptune
Gravitational constant, μ, m^3/sec^2	1.3245×10^{20}	2.23826×10^{13}	3.98604×10^{14}	4.33346×10^{13}	1.30035×10^{17}	3.87446×10^{16}	5.94611×10^{15}	7.05659×10^{15}
Heliocentric orbit radius, m	----------	0.5791×10^{11}	1.4950×10^{11}	2.2779×10^{11}	7.7780×10^{11}	14.2610×10^{11}	28.691×10^{11}	44.956×10^{11}
Heliocentric orbit velocity, m/sec	----------	4.7872×10^{4}	2.97652×10^{4}	2.4130×10^{4}	1.3050×10^{4}	0.9640×10^{4}	0.6780×10^{4}	0.5470×10^{4}
Planet radius, m	----------	2.42105×10^{6}	6.37123×10^{6}	3.33215×10^{6}	6.98925×10^{7}	5.7532×10^{7}	2.3701×10^{7}	2.1535×10^{7}
Sphere-of-influence radius, number of planet radii	----------	47	150	174	690	950	2180	3970
Velocity of circular orbit at 2 planet radii, m/sec	----------	2.150×10^{3}	5.593×10^{3}	2.550×10^{3}	3.050×10^{4}	1.835×10^{4}	1.120×10^{4}	1.280×10^{4}

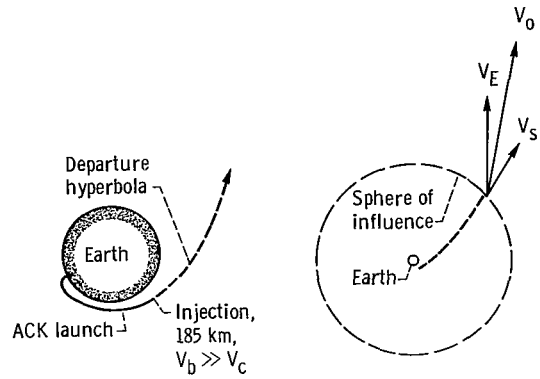

(a)

sultant velocity V_0 is sufficient for the ACK spacecraft to coast on a heliocentric transfer conic section for the remainder of the trip to the target planet. At arrival, the probe spacecraft is on a hyperbolic flyby path inside the planet's sphere of influence. The difference between flyby and capture missions in ACK cases simply depends on whether or not a braking rocket system is carried to be used at periapsis of the encounter hyperbola.

Earth departure of the hyperbolic-electric (HE) missions is very similar to the ACK profile shown in sketch a. For the HE missions an Atlas-Centaur, without the kick stage, is used to launch the solar-electric spacecraft to a velocity V_b at 185 kilometers altitude. The injection velocity is equal to, or greater than, escape velocity ($\sqrt{2}\ V_c$) but is usually much less than the V_b required for ACK missions. The V_b of an HE mission is low because of the effective velocity increment added to the trajectory during the heliocentric electric propulsion phase. As in the ACK mission, at the sphere-of-influence patch point the solar-electric spacecraft velocity V_S is added vectorially to Earth's velocity V_E to determine the initial heliocentric velocity V_0. For HE missions with optimum thrust vector control during the electric propulsion phase in heliocentric space, the optimum orientation of V_S is in the direction of the initial electric thrust vector, as discussed in references 7 to 9.

In the SE electric propulsion mission, the Atlas-Centaur is used to insert the solar-electric spacecraft into a 185-kilometer circular orbit. Then a low-thrust ascending spiral path (using tangential thrust) is followed by the electric spacecraft until Earth escape energy is obtained.

After reaching escape energy on the powered spiral trajectory, it is assumed that the solar-electric spacecraft coasts to the sphere of influence, arriving with a small V_S of about 900 meters per second. This small V_S is optimally added to the vector V_E, as in the HE mission, and a heliocentric electric propulsion phase then follows. A recent publication by Strack (ref. 10) indicates that this velocity addition yields a good approximation to the actual three-body low-thrust Earth escape problem.

The heliocentric electric propulsion trajectory is calculated with a computer code in which optimum thrust vector control is based on the calculus of variations. The typical optimum heliocentric trajectory consists of a single solar-electric propulsion phase of optimum duration, followed by a long coast out to the target planet. The trajectory code is modified for solar-electric propulsion to account for the variation of solar-cell power with distance from the Sun. Figure 1 (from ref. 7) shows the power variation of a typical solar panel used in this report. The underlying numerical analysis for the power profile shown in figure 1 is explained in detail in reference 7. The main factors in figure 1 are the inverse-square variation of solar flux with solar distance and the increase of solar-cell efficiency with decreasing temperature. Decreasing equilibrium temperature of the solar panel beyond 1 astronomical unit (1 AU) allows panel output power to be a larger fraction of the decreasing solar flux. For this example efficiency almost doubles between 1 and 5 AU. The flat portion of the power curve below 0.65 AU is caused by panel tipping to keep the equilibrium temperature constant and output power at its maximum. Above 0.65 AU, the panel is oriented normal to the Sun-spacecraft line. Figure 1 is given only as a typical power profile curve for the purposes of this report. Many similar types of profiles could be constructed with different panel design parameters.

In this study, it is assumed that the ion thrusters operate with variable propellant flow rate to conform to the solar-cell power profile. The jet velocity (specific impulse) of the ion thrusters is assumed to be constant while the total thrust on the spacecraft varies in direct proportion to propellant flow rate. In actual practice, the constant jet velocity, variable thrust operation could be closely approximated by a multithruster array with periodic shutdown of individual thrusters. Multithruster operation with discrete changes in thrust level is, however, not studied in this report.

Chemical Propulsion Systems

Figure 2 summarizes the launch vehicle performance assumed for this report. The figure shows the payload that can be carried to various burnout velocities for three launch systems based on the Atlas booster. These payloads, given for a 185-kilometer (100-n-mi) burnout altitude, are used as the initial mass of all the interplanetary spacecraft in this report.

The lowest curve in figure 2 shows the payload capability of the Atlas-Centaur vehicle alone. The circular orbit payload (5150 kg at a burnout velocity of 7800 m/sec) is used as the initial mass of all SE missions. The Atlas-Centaur curve is also used for two other purposes: (1) to evaluate the initial mass of the electric spacecraft at speeds above escape for the HE-type profile, and (2) to construct the hypothetical kick-stage-performance curve also shown in figure 2.

The highest curve in figure 2 gives the launch payload of the Atlas-Centaur with a

very-high-performance upper stage. This curve is used to give the initial mass of spacecraft for ACK missions. The high-performance kick stage calculated for this report has an assumed specific impulse I_{sp} of 460 seconds and hardware fraction of 20 percent of its propellant load. Details of computing the kick-stage performance are given in appendix C. The performance of the ACK launch vehicle used in this report is extremely optimistic to stress the payload advantage of the solar-electric spacecraft wherever it appears. For comparison, a third curve is given on figure 2 lying midway between the Atlas-Centaur and ACK curves. This middle curve shows the performance of a more realistic kick stage also using hydrogen fluorine (taken from "An Analysis of Chemical Upper Stages for NASA Scientific Missions" by the Staff of Lewis Research Center).

The remaining chemical propulsion system to be mentioned is the braking rocket used in capture missions. This braking rocket is used on both electric propulsion and ACK spacecraft. The braking rocket propellant is assumed to be a storable type with an I_{sp} of 300 seconds. Tankage and other necessary propulsion hardware are assumed to be 20 percent of the braking propellant mass. The amount of braking propellant required will vary from case to case, depending on the ΔV requirement at periapsis of each hyperbolic encounter trajectory.

Spacecraft Descriptions

ACK spacecraft. - Figure 3 is a schematic of the all-chemical-propulsion (ACK) spacecraft; the values used in analyzing the ACK missions are included. The high-performance kick stage is considered a part of the launch vehicle system. The ACK spacecraft is assumed to be made up of a structure framework, a braking rocket system, and the residual payload. The braking rocket system, of course, would not be present in flyby missions. The structure requirement of the spacecraft is assumed to be 10 percent of the total spacecraft mass. This 10 percent structure fraction is somewhat large to provide additional contingency for any other hardware requirements. Subtracting structure and the braking rocket system (if any) from the initial spacecraft mass leaves a residual mass which is called the residual payload. This residual or gross payload must be large enough to include not only scientific instruments but also telemetry, communications powerplant, attitude control, and other necessary subsystems. For the remainder of this report, residual payload will be referred to as payload.

As an example, consider the following calculation of payload for an ACK mission. For a particular mission, a ballistic trajectory calculation might be made which shows that an injection velocity of 14 000 meters per second is required at 185 kilometers (100 n mi) altitude above Earth. In figure 2, the high-performance ACK curve shows

that the spacecraft initial mass M can be 600 kilograms at 14 000 meters per second. If this were an ACK flyby mission, the payload would be 540 kilograms, which is the initial mass reduced by the 10 percent structure allowance. If, however, this were to be an ACK capture mission a propellant requirement for braking the 600-kilogram vehicle at the target planet would be calculated. If this propellant mass is about 100 kilograms, the associated hardware would be taken as 20 percent, or 20 kilograms. The ACK capture mission payload would then be 420 kilograms, since the structure is still 60 kilograms and the braking rocket system requires 120 kilograms of the 600-kilogram spacecraft.

Solar-electric-propulsion spacecraft. - Figure 4 is a schematic of the solar-electric spacecraft given with the weight assumptions used in the mission analysis. Again, as in the ACK spacecraft, the allowance made for structure and any additional hardware contingency is 10 percent of the total mass. It should be noted that, for the electric propulsion spacecraft, this fraction provides a very large contingency for structure and hardware. The total mass is usually larger than an equivalent ACK spacecraft (due to lower injection velocity) and includes a propulsion system mass for which hardware and structure assessments have already been made.

The solar-cell powerplant, consisting of panels and deployment mechanism, is assumed to weigh 50 pounds (23 kg) per kilowatt of output power at Earth's distance (1 AU) from the Sun. This specific weight of the solar-cell powerplant is based on the designs given in reference 1. An additional 25 pounds (11 kg) per kilowatt is charged to the electric spacecraft to account for the weight of ion thrusters and the necessary power regulation equipment. This 25 pounds (11 kg) is made up of an assumed thruster weight of 10 pounds (4 kg) per kilowatt and power conditioning system weight of 15 pounds (7 kg) per kilowatt. The total specific weight of the electric propulsion system α is therefore 75 pounds (34 kg) per kilowatt. The other important subsystem weights accounted for are the weight of propellant and tankage for the ion thrusters and the chemical braking rocket. As in the previously described ACK spacecraft, the residual payload calculated for the solar-electric spacecraft must include many other necessary subsystems. Many of these subsystems, such as attitude and environmental control systems, would be equivalent fractions of either of the solar-electric or ACK spacecraft. A low-power continuous telemetry system would also be a similar additional weight charge to either the solar-electric or ACK spacecraft, since these calculations assume that all available solar-electric-spacecraft primary power is fed to the thrusters. But in coasting periods and on final arrival at the target planet, the solar-electric spacecraft has the potential advantage of using the large main powerplant for increased communication rates and high-power-demand experiments.

Calculation of the maximum payload for the solar-electric spacecraft involves many trade-offs between trajectory requirements and propulsion system design parameters. For this reason, the trajectory code mentioned earlier in this report is incorporated in

a multivariable payload optimization computer code. Weight and performance assumptions for the various spacecraft subsystems are included in the code, such as powerplant specific weight, the effect of injection velocity V_b on spacecraft initial mass, and the variation of thruster efficiency with ion thruster specific impulse.

The ion thrust overall efficiency η is shown in figure 5 as a function of ion thruster specific impulse. The overall efficiency is used in calculating required thruster input power P from the jet power P_j, which itself depends on the thrust F and specific impulse I_{sp} of the ion thrusters

$$P = \frac{P_j}{\eta} = \frac{FI_{sp}g}{2\eta}$$

Powerplant mass of the electric spacecraft is calculated on the basis of 34 kilograms per kilowatt of thruster input power

$$M_{pp} = \alpha P = \frac{34\ P}{1000}$$

The efficiency curve in figure 5 is taken from reference 4 where it is said to be typical of large, 50-centimeter-diameter mercury ion thrusters. However, the comparison points in the figure show that efficiencies of smaller (10 and 15 cm) thrusters of more recent design (ref. 11) can equal or exceed the efficiency of earlier large thrusters. Therefore, the curve is used in this report as typical of a wide range of mercury ion thruster sizes.

RESULTS AND DISCUSSION

Flyby Missions

The only flyby missions studied in this report for payload advantage and/or time savings of the electric spacecraft are those to the Jovian planets (Jupiter, Saturn, Uranus, and Neptune). Performance of the all-chemical (ACK) system is considered to be so superior to HE or SE systems for flybys to Mercury or Mars that comparisons would not be of interest. Jupiter flyby mission results have many characteristics typical of all other mission results to be presented later. Therefore, a more detailed discussion of this case is presented.

High travel angle. - Earlier in this report, the solar-electric-propulsion mission

options were subdivided into SE and HE types. Each of these mission types is now further subdivided into classes that depend on elapsed central angle of the heliocentric trajectory. The reason for this further subdivision is based on the fact that power is supplied by solar cells. It was pointed out in figure 1 that the typical solar panel power drops severely over the range from Earth to Jupiter or the other outer planets. This power loss effect can be offset in many cases by a heliocentric trajectory that, for the same transfer time, spends more time near the Sun by covering a large elapsed central angle.

For a given transfer time, low-thrust heliocentric trajectories often have more than one value of transfer central angle at which the effective value of low-thrust ΔV is a local minimum. However, it has been observed that the magnitude of each local minimum ΔV increases with the local optimum value of transfer central angle. For the outer planets, the lowest value of local minimum ΔV is achieved on trajectories with optimum elapsed central angles of less than 1 revolution about the Sun. In this study, such trajectories are referred to as direct transfers because of the steady increase of solar distance while the solar-electric propulsion system is operating. Two other classes of the trajectory with higher values of local minimum ΔV, but the same transfer time, have elapsed central angles of about 1.5 and 2.5 revolutions, respectively.

Examples of the direct-transfer and 1.5-revolution cases for a 1000-day HE Jupiter flyby are shown in figure 6. The direct trajectory, shown in the left of figure 6, has the lowest effective ΔV. But the higher-travel-angle case, shown in the right of the figure, stays closer to the Sun over a greater portion of the trip and in this way derives more useful solar energy for propulsion with a given weight of solar cells. Note that the high-travel-angle case in figure 6 takes about twice the time to reach 3 AU as the direct-transfer case. Also interesting to note is the excursion taken by the high-travel-angle case out to the vicinity of Mars, inward to the vicinity of Venus, and finally outward to Jupiter. The higher-angle option, covering a wider area of the solar system, could return a large amount of data in addition to its primary mission goal.

In this report the travel-angle class is identified by a suffix A, B, or C. The direct-transfer case is designated SE(A) or HE(A). The higher-travel-angle cases are given two suffixes: (B) for the 1.5-revolution class, and (C) for the 2.5-revolution class. For example, as in figure 6, the HE(A) and HE(B) profiles are the direct-transfer and 1.5-revolution hyperbolic-electric flyby missions. In the close-in solar probe study of reference 7, similar types of high-travel-angle trajectories were found to be desirable for solar-cell-powered electric spacecraft. As in reference 7, this report shows that multirevolution class trajectories are better choices only as relatively longer transfer times are used.

Payload. - Residual payload for the Jupiter flyby mission is given in figure 7 as a function of trip time. Payloads for the solar-electric-propulsion mission options, SE(A), SE(B), HE(A), and HE(B), are shown in comparison with ACK results. The ACK mission

payload curve is shown by a small-dashed line. The Hohmann (minimum high-thrust ΔV) trip time case is indicated at about 1000 days. The ability of the ACK mission mode to deliver more payload at shorter trip times for this mission is quite evident over the whole trip time range. At 1000 days trip time, an additional data point (diamond symbol) is given to show the payload of an ACK mission using the lower performance hydrogen-fluorine kick stage of figure 2. The very flat payload curve over a large trip time range is typical of ACK missions to all four outer planets.

For the solar-electric-propulsion missions, relative performance of each profile option depends on trip time. In general, (B) profiles are better than (A) profiles, and SE cases outperform HE cases as trip time increases. The SE(B) mission profile is the only solar-electric-propulsion case which markedly exceeds the ACK residual payload capability. The advantage of SE over HE profiles disappears at shorter trip times. Also important to note is that the SE profile results shown in this report do not account for a possible power output degradation of the solar cells during the spiral traversal of the Van Allen belt at Earth. A radiation damage weight allowance, especially for silicon cells, would decrease the SE payloads calculated in this study.

Effect of power requirement. - The ACK results given in figure 7 are residual payloads that have not been penalized by any electric-power requirement for communication and scientific instruments at the target planet. If it is assumed that the solar-cell powerplant is usable at Jupiter, the payload comparisons of figure 7 can change. In figure 8 the residual payload of an ACK mission to Jupiter, after subtraction of a powerplant weight allowance, is compared with a few SE and HE results as power requirement at Jupiter is varied. A zero-power payload of 520 kilograms is shown for the best (1000 day) ACK Jupiter flyby (curve taken from fig. 7). The ACK payload in figure 8 (small-dashed line) linearly decreases with increasing power requirement at the rate of 320 kilograms per kilowatt. It is assumed that power for the ACK payload is supplied by a solar-cell panel with the same characteristics as that used in the solar-electric-propulsion vehicle. Figure 1 showed that solar panel output power at Jupiter is about 7 percent of the output at Earth. Solar-cell panels weighing 50 pounds (23 kg) per kilowatt at Earth therefore weigh 705 pounds (320 kg) per kilowatt at Jupiter.

The optimum power level of HE spacecraft in figure 8 is such that nearly 1 kilowatt of power is available at Jupiter. If power needs at Jupiter are about 1 kilowatt or greater, the HE(B) mission shows a definite payload advantage over the ACK mission at 1000 days. Increasing the mission time to 1400 days adds enough payload to nearly equal the zero-power ACK value.

The optimum power level of SE mission spacecraft is about five times the typical HE case. Also, the stronger growth of SE payload with increased trip time is seen by comparing the 350-kilogram 1000-day mission with the 900-kilogram, 1300-day mission. The main reason for large power differences between HE and SE missions is spacecraft size. The SE spacecraft initial weight is equal to the Atlas-Centaur Earth orbit capa-

bility of 5150 kilograms (shown in fig. 2), whereas the typical HE spacecraft is injected at slightly above Earth escape speed with an initial mass of about 1000 kilograms. Both HE and SE spacecraft have a gradual decrease in payload due to off-optimum power. For science power requirements at arrival less than the optimum, it may be best to design the spacecraft for the optimum propulsion power level, and use less of it for science purposes, rather than suffer the payload decrease due to underoptimum power.

Residual payload for the Saturn flyby mission is given in figure 9(a) as a function of trip time. The power output capability of the solar cells is questionable for all planets beyond Jupiter. Therefore, comparisons among different mission modes should be based solely on payload capability without taking into account power that might be available at the planet. Figure 9(a) shows that for Saturn flybys in the low-payload trip time range between 1000 and 1600 days, the ACK mode can deliver higher payloads than are possible with solar-electric propulsion. The HE(A) and SE(A) solar-electric propulsion profiles fall very low in payload capability. However, HE(B) and SE(B) payloads compete with ACK results at trip times that are 400 days shorter than the 2200-day Hohmann case. The 2.5-revolution HE(C) profile begins to show a slight advantage for the Saturn flyby at long trip times. In the following discussion of the Uranus and Neptune flyby cases, the HE(C) profile shows better relative performance over a wider time range.

In figures 9(b) and (c), payloads are shown for various mission profiles for Uranus and Neptune flybys. Note that HE(A) trajectory type results are not shown for either planet. The best HE(A) mission payloads would be less than 100 kilograms for either planet. On the other hand, for both planets, the HE(B) or HE(C) profiles can deliver about twice the ACK payload over a wide range in transfer times. Taken together, figures 7 and 9 clearly show that high-travel-angle trajectories are the most practical choice for missions beyond Jupiter.

As in the Jupiter and Saturn flybys, the SE-type missions deliver the greatest payload if longer trip times are allowed and if spiral Earth escape paths become practical. Data for SE(B) profile results have not been calculated for Neptune. But the Uranus data show that SE(C) and SE(B) profile results are nearly the same except at the longer trip times.

Effect of solar-electric power on system design. - A solar-cell powerplant is lightweight in terms of power output capability at 1 AU. However, the sharp power drop with distance from the Sun introduces an effective penalty on the performance of the solar-electric propulsion system and strongly influences trajectory selection and subsystem weight requirements. Figure 10 is included to help evaluate this power loss effect on solar-cell-powered spacecraft over a range in specific powerplant mass α.

The curves in figures 10(a) and (b) compare the optimum installed power levels, specific impulse, initial mass, and residual payload for a typical mission. The mission used in this example is a 1000-day Jupiter flyby. At each value of α, results typical of a solar-electric-propulsion spacecraft design are compared with those of a spacecraft

having a constant-output electric powerplant. Results for both the direct-transfer HE(A) and high-travel-angle HE(B) profiles are used for the solar-electric curves in figure 10. More complete subsystem breakdowns for the HE(A) and HE(B) 1000-day, solar-electric-propulsion Jupiter flyby cases at an α of 34 kilograms per kilowatt can be compared in table I, which is given in appendix B.

The constant-power data curves are based on the use of a direct trajectory since a constant-power spacecraft would not benefit from the high-travel-angle trajectory option. It is doubtful that constant-power sources can achieve the specific powerplant masses α at the lower end of the range covered in figure 10, except in future systems of high power output. But data are given in this range to allow comparison with results for the relatively lighter solar-cell powerplant. The solid symbols on the curves at α of 34 kilograms per kilowatt mark the payload, initial mass, specific impulse, and installed power of the solar-electric HE(A) and HE(B) reference cases taken from figure 7. It can be seen in figure 10 that for either constant or solar-electric power the installed power level, specific impulse, initial mass, and payload decrease with increasing α. The trends of the constant and solar power data are similar.

For either the HE(A) or HE(B) solar-electric mission profiles, the payload decrease from the constant-power case is about the same at each α. Above α of 50 kilograms per kilowatt, the HE(A) profile results in greater payload than the HE(B) for this mission.

The values of optimum specific impulse of the solar-electric cases are lower than those of the constant-power system at any value of α. This is due to solar power drop-off, which has the effect of shortening the useful propulsion time. Also, the decreasing solar power during the propulsion period has the effect of increasing the α of the solar power system relative to its value at 1 AU. Of the solar-electric propulsion cases, optimum specific impulse is generally lowest at each α for HE(A) mission profiles because of the more rapid movement of an HE(A) trajectory outward from the Sun.

Compared with constant-power results, optimum solar-electric spacecraft designs for either the HE(A) or HE(B) mission profiles require a larger fraction of the spacecraft to be devoted to powerplant. Also, solar-electric missions often require higher launch velocities from the launch vehicle and, as a result, have lower total spacecraft mass than constant-power cases. Any optimum design for the HE(B) solar-electric mission shown in figure 10 has an initial spacecraft mass very close to that of the constant-power case. However, the solar-electric design calls for 1 to 2 kilowatts more installed power than the constant-power case at most values of α. Moreover, due to the high ΔV requirement of type-B mission trajectories, an additional large fraction of the HE(B) spacecraft is needed for the propellant. Therefore, the combined effects of increased powerplant and propellant mass for the HE(B) mission profile significantly reduce payload capability.

Due to a rapid loss of solar power, spacecraft designs for an HE(A) solar-electric mission call for a high value of the ratio of installed power to initial mass. Yet the HE(A) results in figure 10 show an optimum power level that is less than for HE(B) or constant-power requirements over a large range of α. Also, it is usually observed that for direct trajectories the ΔV, and therefore the required propellant fraction, of the solar-electric spacecraft is small and decreases further as α is increased. Payload continues to decrease in the HE(A) mission, in spite of decreased powerplant mass and propellant mass, because of the decrease in spacecraft initial mass. The low initial mass, which results from high required values of launch velocity in HE(A) missions, decreases more rapidly than the powerplant and propellant mass as α is increased. Hence, the principal cause of low payload in HE(A) solar-electric missions is low total spacecraft mass.

To summarize, the power drop of the solar-cell system has two dominant effects on spacecraft performance for either direct or high-travel-angle trajectories. First, the installed weight of powerplant must be high so that a useful average power level is available for propulsion. Second, the drop in thrust with power to very low levels early in the mission trajectory greatly decreases useful propulsion time. The shorter effective propulsion time (or higher effective α) calls for lower specific impulse and, therefore, higher propellant fraction than a constant-power system would need.

Finally, as shown in figure 10, if a constant-output-power system could be built at an α of 50 kilograms per kilowatt, its payload would only slightly exceed the payload of the solar-electric reference case at α of 34 kilograms per kilowatt. A 3500-day Uranus flyby, which also has a payload of about 300 kilograms at an α of 34 kilograms per kilowatt, was similarly examined to compare constant and solar power at various values of α. The comparisons between constant-power and HE(B) solar-electric results were found to be nearly the same as those shown in figure 10 for the 1000-day Jupiter mission. Therefore, if given enough transfer time, the only apparent serious penalty connected with the use of solar-cell power is that the powerplant may not be usable at planets beyond Jupiter.

Effect of propulsion time. - Figure 11 shows the effect of allowed propulsion time on payload for 1000-day Jupiter and 3500-day Uranus flyby missions. Figures 7 and 9 show that trip times to the outer planets are very long for either chemical propulsion or solar-electric propulsion spacecraft. Many important components of either spacecraft will need a high life expectancy if the probe mission is to be a success. A long-life ion thruster system is one component needed for the electric spacecraft that, of course, is not needed for the ACK spacecraft. However, because of the rapid fall-off of solar power, most of the propulsion work of the ion thrusters is complete by the time the spacecraft reaches a distance of about 3 AU. It has been found that, even for very lengthy trips, propulsion times can be reduced to 1000 days or less for a small penalty in payload. For the Jupiter flyby, curves are shown in figure 11 for both the HE(A)

direct-transfer and HE(B) 1.5-revolution profiles. The Uranus curve shows only the HE(B) case because the HE(A) profile payload is far too small. All three payload curves show an optimum propulsion time and a fairly rapid payload loss if propulsion time is overly shortened. But a propulsion time as short as 800 days can be used for the Uranus mission for a payload loss of less than 20 percent of the maximum. A propulsion time of 800 days is optimum for the HE(B) Jupiter mission and this trip can be cut to 500 days of propulsion for a payload loss of less than 20 percent. Of course, if propulsion time must be limited to 500 days or less, the HE(A) profile is the best choice for the Jupiter mission. A propulsion time of no more than 500 days would be sufficient for HE(A) profiles to all the outer planets. But is should be remembered that, compared to the HE(B) profile, the HE(A) profile has a very poor payload capability for all planets beyond Jupiter. The HE(B) profiles need more propulsion time than the HE(A) cases because of their extra loop around the Sun. However, only about 800 days would be necessary for a payload loss of less than 20 percent on most HE(B) missions. The HE(C), 2.5-revolution profile is the best choice for many Uranus and Neptune missions. But propulsion times of about 1200 days are necessary for the HE(C) trips or their payload advantage over HE(B) profiles is lost.

It should also be noted that the propulsion times discussed herein are not necessarily the required operating lifetimes of the ion thrusters. Figure 12 shows the propulsion power variation along the trajectories of the three cases shown in figure 11. The two Jupiter examples are an HE(A) trajectory with 300 days allowed propulsion time and an HE(B) trajectory with 600 days of propulsion. The third curve in figure 12 shows the propulsion power history of a 3500-day Uranus flyby with 800 days propulsion time. The combined effects of the variation of solar power with radius and radius with time along each trajectory type produce the power curves seen in figure 12. For a multi-thruster electric spacecraft, the power variation means that, for most of the propulsion time, the required number of operating thrusters is less than the number on board. The solar-electric spacecraft therefore has a built-in redundancy which may be used to advantage for high reliability beyond the expected life of individual thrusters. For example, in all three cases shown in figure 12 there are only short time periods during which all the thrusters must operate. Also, for the HE(B) Jupiter and Uranus missions, there are only 350 days during which more than half of the thrusters must operate.

Minimum trip time for fixed payload. - Figures 7 and 9 show that solar-electric-propulsion payload capability is essentially the same for all four Jovian planets. The major difference between solar-electric-propulsion missions to each planet lies in the transfer time required to deliver a specific payload level. On the other hand, the ACK mission falls behind in payload against time capability as more distant target planets are selected. These comparisons of payload and time requirement for outer planet flybys are summarized in figure 13.

Figure 13 shows the minimum time required to deliver specified payloads to the four Jovian planets as a function of the distance of the planet from the Sun. For solar-electric-propulsion missions, 200-, 300-, and 400-kilogram HE payload curves are shown, along with an 800-kilogram SE mission curve. Only the 200- and 300-kilogram ACK mission payload curves are shown in figure 13 since payloads of 400 kilograms or greater are not possible for planets beyond Jupiter. Comparing the small-payload (200 kg) ACK and HE curves shows that shorter mission times are possible with the ACK spacecraft for Jupiter and Saturn. Figures 7 and 9(a) show that the ACK time advantage continues to hold at Jupiter for payloads as large as 500 kilograms, but vanishes at Saturn or beyond for payloads over 300 kilograms. For Uranus and Neptune, the 200-kilogram HE curve outperforms the ACK mission by a very large margin. Also interesting to note is that for a 200- to 250-kilogram payload, the HE spacecraft has about the same design parameters for all four outer planets. Data given in tables II and III of appendix B show that total installed power is about 10 kilowatts, that mercury ion thrusters should operate at an I_{sp} of 4000 to 5000 seconds, and that the initial mass of the solar-electric spacecraft is about 1000 kilograms. These values illustrate the multimission capability that solar-electric propulsion could provide in a one-design spacecraft.

The SE mission curve for 800 kilograms payload is included in figure 13 to illustrate the high payload potential of this mode if the technical problems associated with Earth escape spirals and high spacecraft installed power (about 50 kW) can be overcome. Note that the 800-kilogram SE mission can be completed in mission times equal to or less than that for the 400-kilogram HE mission. The SE mission mode is, however, best suited to high payload requirement. A 200-kilogram SE payload curve would have about the same minimum times as the payload curve shown for the 200-kilogram HE mission, because of the steep slope of the SE payload curves shown in figures 7 and 9.

Capture Missions

In this final section, capture mission payloads for Jupiter, Saturn, Uranus, Neptune, Mars, and Mercury are presented in the same way that flyby results were given in the previous section. As mentioned in the ANALYSIS section, the final parking orbit for all planets is highly elliptical with a periapsis of 2 planet radii. This type of capture orbit results from high thrust braking of the spacecraft to just below escape velocity at the desired periapsis radius. Higher periapsis radii or lower eccentricity parking orbit requirements would increase the braking ΔV and, therefore, reduce the payload.

Jupiter and Saturn. - Figures 14(a) and (b) show residual payloads for the ACK, SE, and HE capture missions to Jupiter and Saturn. For Jupiter (fig. 14(a)), the relative

performance level of each of the various mission profiles is much the same as that of the previous flyby data of figure 7. However, each solar-electric-propulsion capture mission requires about 300 days additional time to equal the flyby payloads. The HE capture mission payloads are 50 to 150 kilograms less than the flyby payloads at each trip time. The difference between flyby and capture payloads for SE missions is about 400 kilograms. The ACK capture results show a small payload decrease (about 100 kg) from the flyby values at each trip time.

The Jupiter capture data are based on high thrust braking of the entire electric spacecraft (structure, powerplant, and payload) upon arrival at periapsis. For Saturn captures (fig. 14(b)), this mode of operation results in negligible payloads below trip times of 2400 days. No payload is possible for the HE mission profile when the whole spacecraft is captured. The SE(B) profile, a small section of which is shown in figure 14(b), has a 120-kilogram payload at 2400 days.

Payload separation. - The other SE and HE Saturn capture curves in figure 14(b) are labeled "SPLIT." The SPLIT designation means that the payload package (with the braking rocket) is first separated from the main spacecraft before the capture braking maneuver. The basic reason for this separation is that the solar-cell powerplant, and its associated systems, is almost useless at Saturn and therefore constitutes a large "deadweight" penalty on the electric spacecraft during the braking maneuver. Even if the solar cells functioned at twice their Earth efficiency, their equivalent weight at Saturn's distance from the Sun would be 1200 kilograms (~2600 lb) per kilowatt. A radioisotope power system would probably weigh less than half this amount. Therefore, the payload is separated from the main spacecraft to reduce the mass which must be decelerated at periapsis by the small high-thrust capture system.

The curves for Saturn in figure 14(b) show that the SPLIT concept greatly increases net delivered payload. This increase can be seen by comparing, at 2400 days, the SE(B) and SE(B) SPLIT payloads. Relative performance comparisons of SPLIT solar-electric-propulsion missions and ACK results now depend solely on net delivered payload and/or time requirements. For either of the two systems, communication power would have to be carried as part of the payload. It can be seen that, at Saturn, the payload capability of the SPLIT solar-electric spacecraft exceeds the ACK payload capability only for long trip times. Only the SE(B) SPLIT case appears to have the ability to deliver payloads much heavier than the ACK. The HE(B) and HE(C) SPLIT curves show a much smaller gain over the ACK results.

Uranus and Neptune. - In figure 14(c) for Uranus, and figure 14(d) for Neptune, capture payloads for SPLIT solar-electric-propulsion mission profiles are compared with ACK results. The all-chemical-propulsion ACK mission profile payloads fall to very low levels for these missions. Comparison with figures 14(a) and (b) shows that the general trend of the ACK performance is similar to that of the flyby data of figures 7 and 9. Maximum payload capability steadily decreases and trip time requirement in-

creases. On the other hand, the HE and SE capture mission results seen in figures 14(a) to (d) show that, although trip time requirement increases, the payload does not decrease at as rapid a rate as the ACK cases. Also, as was true in the flyby case, the HE(B), HE(C), and SE(C) multirevolution profiles make the best use of the solar-electric power-plant for these distant planet missions.

Mars and Mercury. - Data for Mars and Mercury capture missions are included in this report because, for different reasons, these cases provide an interesting extension to the capture and flyby data given for the four Jovian planets. The Mercury and Mars cases shown here are not SPLIT missions. For both planets, the payloads shown in figure 14(e) are for high-thrust braking of the entire spacecraft at periapsis, as in the Jupiter capture data of figure 14(a). The reason for this is that the solar cells have a very good output power capability at both planets and probably should not be discarded, provided that all the power can be used. In the Mars mission special high-travel-angle trajectory options have not been used and are probably not necessary since solar-cell power loss between Earth and Mars is only about 50 percent. As with Jupiter, the direct-transfer (or (A)) trajectories to Mars require between 1/2 and 1 revolution about the Sun. However, for the Mercury cases shown here, the best trajectories for solar-electric propulsion take between 2 and 3 loops around the Sun, and solar power actually increases during the mission.

Payload capabilities for Mars and Mercury missions are sensitive to synodic period (launch year) effects because of the relatively high eccentricity of the solar orbits of these two planets. In general, better payloads for both electric propulsion and ballistic missions are possible when the spacecraft encounter occurs at Mars' perihelion or at Mercury's aphelion. However, the results presented in figure 14(e) are based on the assumption that Mars and Mercury are in circular heliocentric orbits at their respective mean distances given in table I. This mean orbit assumption reliably indicates the average payload capability between the best and worst synodic periods.

The Mars mission might be interesting as a test mission for later probes to the Jovian planets. Initial mass of the electric spacecraft is about 1000 kilograms, as in the Jupiter missions. But required installed power and trip time are about one-half the values needed for the Jupiter flyby or capture missions. If the Mars capture is weighed on its own merits, payload capability of the solar-electric spacecraft is inferior to ACK capability. However, the difference between ACK and solar-electric payload results can be offset by mission objectives which require a high power in Mars orbit such as additional electric propulsion maneuvers or high data rate telemetry.

Payloads for a solar-electric-propulsion Mercury mission are of interest because Mercury capture is not possible at all with the ACK system. High-thrust trajectories to Mercury have very high approach velocities and, therefore, extremely high ΔV requirements for the periapsis braking maneuver. With all-chemical propulsion, reasonable payloads could only be delivered to a Mercury parking orbit with very large

launch boosters at Earth and multistage braking at Mercury. With a solar-electric-propulsion spacecraft and the Atlas-Centaur launch vehicle, about 300 kilograms of payload could be captured for a trip time of 500 days. The electric spacecraft would again have about the same initial mass and installed power as needed for the Jovian planet missions. Furthermore, due to expected power gain of the solar cells (see fig. 1), between 14 and 17 kilowatts could be available for communications and science experiments while in the Mercury parking orbit.

CONCLUDING REMARKS

This preliminary study was conducted to identify the best trajectories and propulsion system design parameters for a solar-electric spacecraft over a wide range of interplanetary missions. Special trajectories which include a gravity assist or swingby at an intermediate planet were excluded from this study. The payload capability of the solar-electric-propulsion spacecraft were also compared with a high-performance, all-chemical-propulsion method of carrying out each mission. Comparisons were made on the basis of gross or residual payload (spacecraft arrival mass minus structure and propulsion system mass) delivered to each planet on flyby and loose elliptical planetary capture missions. Data of the type presented, such as desired power level and specific impulse, can help direct research and development efforts for solar-electric propulsion system components. Such data, in combination with other studies such as development cost and reliability, would help determine the desirability of solar-electric propulsion for probe missions.

The results presented for both all-chemical and solar-electric propulsion systems are based on the Atlas-Centaur launch booster. Trajectory and propulsion system parameters were optimized for probe spacecraft to match this particular launch vehicle. For other launch boosters such items as payload and required power level can be estimated by scaling. The scale factor is the ratio, between Atlas-Centaur and the other launch booster, of initial mass of the probe spacecraft at the injection velocity required for each mission.

The Atlas-Centaur and solar-electric spacecraft combination of this study can deliver at least 300 kilograms of gross payload to Jupiter, Saturn, Uranus, and Neptune on HE-type flyby missions. For the same four planets, HE-type capture missions can place at least 200 kilograms of payload in elliptic parking orbit. Comparisons with the ACK results show that, from Jupiter to Neptune, HE mission payloads drop at a much lower rate from planet to planet than those of similar all-chemical-propulsion missions. Mars capture capability, while less than the ACK results shown in this study, is 700 kilograms for mission times above 300 days. Solar-electric Mercury capture missions have a

distinct advantage over the ACK system since all-chemical-propulsion Mercury captures are nearly impossible.

If Earth escape spirals and larger power levels become more feasible for solar-electric propulsion, the SE mission profiles are shown to have the highest payload capability of all systems based on the same launch vehicle. Payloads of 10 to 20 percent of the Atlas-Centaur orbital capability (5150 kg) are possible.

For reasonable payload levels to the outer planets with systems based on Atlas-Centaur, required transfer times are often very long regardless of whether all-chemical- or solar-electric-propulsion mission profiles are used. For example, transfer times for Jupiter missions lie between 1.5 and 3.5 years, and trips to Neptune take 10 to 14 years. Such lengthy trips are probably the most severe detriment to the prospect of any missions to the outer planets. However, even for the most lengthy mission times, long propulsion times are not necessary for the solar-electric spacecraft. Due to the dropoff of solar power with distance from the Sun, propulsion cutoff times can be shortened to 1000 days or less for small penalties in payload. The solar power drop along each trajectory also helps to decrease propulsion lifetime requirements of the ion thrusters.

Taken overall, the comparisons in this study do not make a strong case for choosing solar-electric propulsion over advanced all-chemical systems, despite the omission from the analysis of various possible practical constraints such as thruster lifetime, simpler nonoptimum thrust vector control, or solar panel orientation requirements. For only a few cases, Mercury capture and long missions to Uranus and Neptune, has solar-electric propulsion shown a definite performance edge over the all-chemical systems. But it should be pointed out that the high-thrust performance used in this study lies close to the upper theoretical limit of chemical propulsion. Solar-electric propulsion systems, on the other hand, have a great potential for improvement in the performance and weight of thrusters and power sources.

Lewis Research Center,
National Aeronautics and Space Administration,
Cleveland, Ohio, March 27, 1969,
789-30-01-01-22.

APPENDIX A

SYMBOLS

F	thrust, N
f_k	$1.2\exp(-\Delta V_k/I_{sp}g) - 0.2$
g	standard gravity, 9.80665 m/sec^2
I_{sp}	specific impulse, sec
M	total or initial mass of spacecraft at Earth escape, kg
M_c	power conditioning and regulation system mass, kg
M_e	engine mass, kg
M_h	hardware mass, chemical braking rocket system, kg
M_{he}	ion thruster hardware and tankage, kg
M_k	payload mass caried by Atlas-Centaur, kg
M_l	gross or residual payload, kg
M_p	propellant mass, chemical braking rocket system, kg
M_{pe}	propellant mass, ion electric propulsion system, kg
M_{pp}	solar-cell powerplant mass, kg
M_{st}	structure mass, kg
P	thruster input power, W
P_j	jet or beam power, W
T	total travel time or trip time, days
T_P	propulsion time, days
V_b	launch or injection velocity, m/sec
V_c	circular orbit velocity, m/sec
V_E	heliocentric velocity of Earth, m/sec
V_o	initial heliocentric velocity of spacecraft, m/sec
V_s	velocity of spacecraft relative to Earth at sphere of influence, m/sec
ΔV	characteristic velocity increment, m/sec
ΔV_k	kick-stage velocity increment, m/sec
ΔV_t	total burnout velocity increment above circular speed
α	electric propulsion system specific powerplant mass, kg/kW
η	overall efficiency of ion thrusters
μ	gravitational constant, m^3/sec^2

APPENDIX B

SUMMARY OF SYSTEMS AND DESIGN PARAMETERS FOR SOLAR-ELECTRIC MISSIONS

This appendix presents more complete descriptions of the optimally designed solar-electric spacecraft for each of the missions analyzed in this report. Data are given in table II for flyby missions and table III for the capture missions. Examples are given for both the hyperbolic-electric (HE) missions and spiral-electric (SE) missions. As stated in the main body of this report, the capture missions are calculated for a highly elliptical capture orbit (just below escape energy) at each planet with a periapsis of 2 planet radii.

In both tables II and III, the first six columns give mission and trajectory information such as trip time, heliocentric travel angle, and optimum injection velocity of the electric spacecraft at 185 kilometers altitude. The next several columns give the spacecraft initial mass and the mass of each of the major subsystems. The last four columns give the optimum installed power, thrust, and specific impulse for the ion thrusters, with the corresponding value of overall thruster efficiency.

The injection velocity for all the SE-type missions is given as 7800 meters per second, which is taken to be the circular orbit velocity at 185 kilometers altitude. In these cases, initial mass of the electric spacecraft is always 5150 kilograms. For SE cases, total travel time is always greater than the heliocentric travel time because of the time spent on the Earth escape spiral. Injection velocity for HE-type missions varies from case to case, since it is optimized to maximize delivered payload. Spacecraft initial mass for HE missions varies with injection velocity, and in all cases is about 1200 kilograms or less.

To illustrate the effect of mission profile type on spacecraft design, data are given for both the HE(A) and HE(B) mission profiles for a 1000-day Jupiter flyby (in table II) and a 1200-day Jupiter capture (in table III). In general, the type-B high-travel-angle profile has a lower optimum injection velocity but higher values of initial mass, propellant, and optimum specific impulse. For example, in the 1000-day Jupiter flyby mission, the HE(A) profile calls for an injection velocity of 11 482 meters per second, whereas the same mission with an HE(B) profile optimizes at an injection velocity of only 11 150 meters per second. In general, higher-travel-angle trajectories allow longer times for the solar-electric propulsion system to do useful work. For this reason, as type A, B, and then C profiles are used, optimum specific impulse increases and the ratio of thrust to initial mass decreases.

The Saturn, Uranus, and Neptune capture mission data given in table III are for SPLIT missions, where only the payload is left in elliptic capture orbit. For some of the missions in table III, the braking rocket system mass requirement was so small that it was arbitrarily specified at 10 kilograms.

TABLE II. - SUMMARY OF SYSTEMS FOR FLYBY MISSIONS

Target planet	Trajectory					Mass allocation, kg					Propulsion system			
	Heliocentric travel time, days	Total travel time, days	Mission profile type[a]	Heliocentric travel angle, deg	Injection velocity at 185 km, m/sec	Initial mass	Structure	Powerplant power conditioning thrusters	Propellant and tankage	Residual payload	Total power at 2 AU, kW	Thrust at 1 AU, N	Ion specific impulse, sec	Thruster overall efficiency, η
Jupiter	800	800	HE(A)	215	11 607	807	81	308	185	232	9.0	0.334	3440	0.62
	1000	1000	HE(A)	240	11 482	896	90	334	207	265	9.8	.356	3820	.65
	1000	1000	HE(B)	496	11 150	1143	114	372	365	293	10.9	.345	4560	.71
	1200	1200	HE(B)	538	11 137	1155	115	340	290	408	10.0	.293	5150	.74
	1400	1400	HE(B)	562	11 130	1160	116	318	255	471	9.3	.273	5200	.74
	800	990	SE (A)	265	7 800	5150	515	2080	2201	354	61.0	2.11	4000	.68
	1000	1283	SE (B)	510	7 800	5150	515	1700	2035	900	49.9	1.433	5340	.75
Saturn	1600	1600	HE(B)	526	11 194	1110	111	378	366	254	11.1	0.338	4850	0.72
	2000	2000	HE(B)	566	11 171	1134	113	358	300	362	10.5	.296	5520	.76
	2600	2600	HE(C)	862	11 109	1180	118	313	311	438	9.2	.228	6670	.81
	1400	1652	SE (B)	516	7 800	5150	515	1785	2480	370	52.4	1.655	4560	.71
	1700	1996	SE (B)	563	7 800	5150	515	1660	2167	806	48.8	1.370	5530	.76
Uranus	3000	3000	HE(B)	552	11 265	1060	106	358	343	256	10.5	0.306	5200	0.74
	4000	4000	HE(C)	851	11 204	1110	111	322	293	354	9.5	.237	6570	.81
	5000	5000	HE(C)	870	11 211	1108	111	293	266	410	8.6	.211	6760	.82
	2500	3079	SE (B)	585	7 800	5150	515	1870	2145	620	54.9	1.463	6010	.79
	3500	3865	SE (C)	830	7 800	5150	515	1440	2235	960	42.3	1.122	6060	.79
Neptune	4000	4000	HE(B)	530	11 450	928	93	321	314	200	9.4	0.281	5000	0.73
	5000	5000	HE(C)	846	11 168	1134	113	347	364	310	10.2	.261	6350	.80
	8000	8000	HE(C)	860	11 230	1092	109	305	300	378	9.0	.223	6700	.82
	3800	4111	SE (C)	816	7 800	5150	515	1585	2655	395	46.5	1.305	5550	.76
	5200	5553	SE (C)	832	7 800	5150	515	1570	2154	911	46.1	1.166	6510	.81

[a]Hyperbolic-electric (HE) type uses Atlas-Centaur booster to launch electric spacecraft to escape velocity or higher at start of mission. Spiral-electric (SE) type uses low-thrust electric propulsion spiral path to escape Earth from low circular orbit. A, direct-transfer case; B, 1.5-revolution high-travel-angle case; and C, 2.5-revolution high-travel-angle case.

TABLE III. - SUMMARY OF SYSTEMS FOR ELLIPTICAL CAPTURE MISSIONS

Target planet	Trajectory						Mass allocation, kg						Propulsion system			
	Heliocentric travel time, days	Total travel time, days	Mission profile type[a]	Heliocentric travel angle, deg	Injection velocity at 185 km, m/sec	Approach velocity at planet, m/sec	Initial mass	Structure	Powerplant power conditioning thrusters	Propellant and tankage	Braking rocket system	Residual payload	Total power at 1 AU, kW	Thrust at 1 AU, N	Ion specific impulse, sec	Thruster overall efficiency, η
Mercury	400	400	HE	876	11 176	627	1130	113	444	350	10	213	13.0	0.376	5300	0.75
	500	500	HE	1062	11 025	630	1246	125	437	352	10	322	12.8	.344	5960	.78
	400	660	SE	835	7 800	628	5150	515	1766	2270	10	589	51.8	1.542	5040	.74
Mars	280	280	HE	195	11 194	1720	1112	111	108	66	150	677	3.2	0.115	3550	0.63
	400	400	HE	276	11 047	545	1226	123	191	118	10	784	5.6	.181	4410	.70
	250	539	SE	184	7 800	1825	5150	515	1549	1298	627	1161	45.5	1.361	5000	.73
Jupiter	1000	1000	HE(A)	229	11 742	4022	731	73	241	177	29	211	7.1	0.258	3540	0.63
	1200	1200	HE(A)	262	11 478	~3600	908	91	321	229	20	247	9.4	.339	3660	.64
	1200	1200	HE(B)	505	11 158	~6300	1140	114	316	372	116	222	9.3	.306	4260	.69
	1400	1400	HE(B)	542	11 133	~5100	1162	116	340	268	93	345	10.0	.288	5300	.75
	1200	1423	SE (A)	321	7 800	3075	5150	515	1900	2180	61	494	55.8	1.782	4480	.70
Saturn	2000	2000	HE(B)	548	11 149	7470	1148	115	374	335	114	210	11.0	0.314	5400	0.76
	3000	2000	HE(C)	858	11 055	4779	1220	122	339	333	67	359	10.0	.247	6680	.81
	2100	2425	SE (B)	582	7 800	7036	5150	515	1640	1910	340	745	48.1	1.263	6150	.79
Uranus	4500	4500	HE(B)	582	11 207	5642	1102	110	354	322	106	210	10.4	0.290	5590	0.76
	6000	6000	HE(C)	867	11 173	4231	1133	113	316	317	80	307	9.3	.230	6690	.81
	4000	4371	SE (C)	838	7 800	8084	5150	515	1545	2020	618	452	45.4	1.115	6790	.82
Neptune	6000	6000	HE(C)	854	11 173	8700	1133	113	328	348	199	145	9.6	0.247	6370	0.80
	8000	8000	HE(C)	869	11 210	5367	1100	110	309	302	104	275	9.1	.222	6810	.82
	6000	6360	SE (C)	837	7 800	7943	5150	515	1595	2055	510	475	46.9	1.150	6800	.82

[a]Hyperbolic-electric (HE) type uses Atlas-Centaur booster to launch electric spacecraft to escape velocity or higher at start of mission. Spiral-electric (SE) type uses low-thrust electric propulsion spiral path to escape Earth from low circular orbit. A, direct-transfer case; B, 1.5-revolution high-travel-angle case; and C, 2.5-revolution high-travel-angle case.

The optimal design parameters and subsystem allocations shown in tables II and III apply only to the specific vehicle analyzed in this report. Any changes in powerplant specific mass, launch vehicle, or ion thruster efficiency would change the table values if the payload optimization procedure was repeated. Nonoptimum, but valid, estimates of the effect of a change in launch vehicle can be obtained by direct scaling. First, a value of solar-electric spacecraft initial mass for the new launch vehicle is found for the table values of injection velocity. Then all subsystem masses, including payload, and the total power and thrust requirement can be scaled by the ratio of initial mass for the new booster to the initial mass given in the table for the system based on Atlas-Centaur.

APPENDIX C

PERFORMANCE CALCULATIONS FOR HYPOTHETICAL KICK STAGE

Calculation of the kick-stage performance for this report is a simple procedure based on the ideal rocket equation. In these calculations, payload of the Atlas - Centaur - kick stage combination is calculated as a function of the total burnout velocity increment above circular speed ΔV_t. The ΔV_t is assumed to be made up of two parts: ΔV_c contributed by Atlas-Centaur and ΔV_k contributed by the kick stage. For the maximum payload at each ΔV_t, the optimum pair of ΔV_c and ΔV_k should be found.

The gross payload M_l to be given a velocity increment ΔV_t is the payload mass carried by the Atlas-Centaur M_k minus the kick-stage propellant, hardware, and engine mass

$$M_l = M_k - M_p - M_h - M_e \tag{C1}$$

where M_p, M_h, and M_e are the kick-stage propellant, hardware, and engine masses, respectively. In this case the propellant depends on ΔV_k and the assumed value of 460 seconds for the specific impulse I_{sp}. Hardware, to account for tankage and structure, is assumed to be 20 percent of the propellant. Engine mass for this size of kick stage is assumed, for simplicity, to be held at a minimal value of 70 kilograms. For convenience in the analysis, equation (C1) is rewritten as

$$M_l = M_k f_k - 70 \tag{C2}$$

where

$$f_k \equiv 1 - 1.2 \frac{M_p}{M_k} = 1.2 \exp\left(\frac{-\Delta V_k}{I_{sp} g}\right) - 0.2$$

and M_e is set at 70 kilograms. The parameter f_k accounts for the hardware percentage and the effect of ΔV_k and I_{sp} on propellant. Values of f_k at each ΔV_k are plotted in figure 15 for $I_{sp}g$ equal to 4511 meters per second.

Maximizing M_l is a matter of maximizing the product $M_k f_k$ in equation (C2). However, M_k depends on ΔV_c, the velocity increment given to the kick stage by Atlas-Centaur. Values of M_k as a function of ΔV_c are given in figure 16. Figure 16 is taken directly from figure 2. For each ΔV_t, varies ΔV_c values are picked to determine M_k. Each ΔV_c also determines ΔV_k and, therefore, the value of f_k. The

maximum product $M_k f_k$ is then found for each ΔV_t. Subtracting the 70-kilogram engine mass from the maximum $M_k f_k$ yields the best M_l for that ΔV_t.

For example, for a ΔV_t of 5000 meters per second, these steps are shown in the following table:

Contribution to velocity increment by Atlas-Centaur, ΔV_c, m/sec	Payload mass carried by Atlas-Centaur, M_k, kg	Kick-stage velocity increment, ΔV_k, m/sec	Parameter, f_k	Gross or residual payload, M_l, kg
1200	3350	3800	0.318	995
1300	3240	3700	.330	1000
1400	3100	3600	.340	985
1500	2970	3500	.352	975

The best gross payload in this example is 1000 kilograms for a ΔV_t of 5000 meters per second. The optimum ΔV_c is 1300 meters per second, and optimum Atlas-Centaur payload M_k is 3240 kilograms. This procedure, repeated for several values of ΔV_t, generates the kick-stage curve in figure 16 and figure 2 of the main text.

REFERENCES

1. Ratcheson, William I.: Fabrication Feasibility Study of a 20 Watt Per Pound Solar Cell Array. Rep. D2-23942-5, Boeing Co. (NASA CR-70582), Nov. 19, 1965.
2. Potter, Andrew E., Jr.: Conventional and Thin-Film Solar Cells. Space Power Systems Advanced Technology Conference. NASA SP-131, 1966, pp. 53-72.
3. Ernsberger, G. W.; and Stechschulte, D. L.: Power Conditioning and Control System for An Ion Thrustor. Rep. WAED-66.59E, Westinghouse Electric Corp. (NASA CR-54672), Nov. 1966.
4. Reader, Paul D.: Experimental Performance of a 50 Centimeter Diameter Electron-Bombardment Ion Rocket. Paper 64-689, AIAA, Aug. 1964.
5. Moeckel, W. E.: Promises and Potentiallities of Electric Propulsion-Status of Thrustor Performance. Paper 66-1024, AIAA, Dec. 1966.
6. Molitor, J. H.; and Olson, R. N.: Solar-Electric Propulsion Systems for Unmanned Space Missions. Paper 67-713, AIAA, Sept. 1967.
7. Strack, William C.: Solar-Electric Propulsion System Performance for a Close Solar Probe Mission. J. Spacecraft Rockets, vol. 4, no. 4, Apr. 1967, pp. 469-475.
8. Strack, William C.: Combined High-Low Thrust Propulsion for the Close Solar Probe Mission. NASA TN D-3145, 1965.
9. Horsewood, J. L.: Interplanetary Trajectory Analysis for Combined High- and Low-Thrust Propulsion Systems. American Astronautical Society Space Flight Mechanics Specialists Symposium. Vol. 11 of AAS Science and Technology Series. M. L. Anthony, ed., American Astronautical Society, 1967, pp. 457-476.
10. Strack, William C.: Some Numerical Comparisons of Three-Body Trajectories with Patched Two-Body Trajectories for Low Thrust Rockets. NASA TN D-4559, 1968.
11. Margosian, Paul M.: Preliminary Tests of Insulated Accelerator Grid for Electron-Bombardment Thrustor. NASA TM X-1342, 1967.

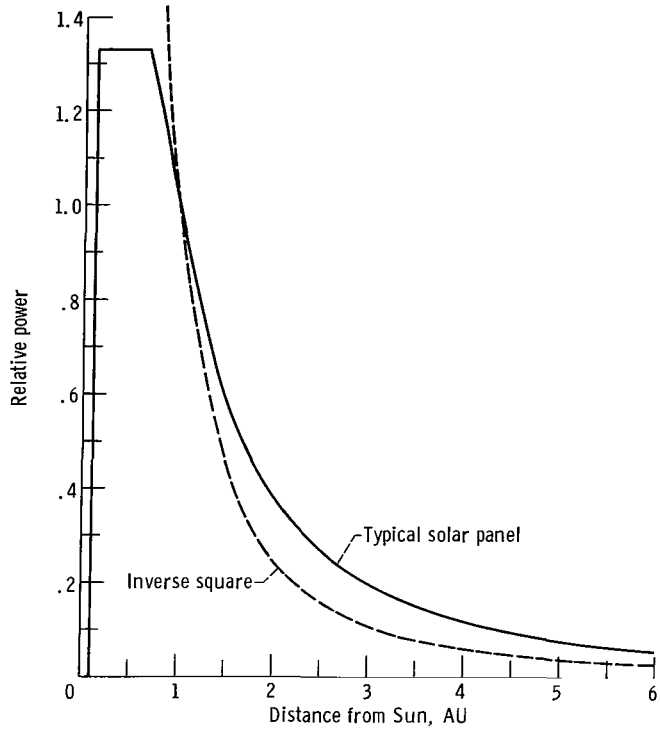

Figure 1. - Effect of distance from Sun on typical solar-cell panel output.

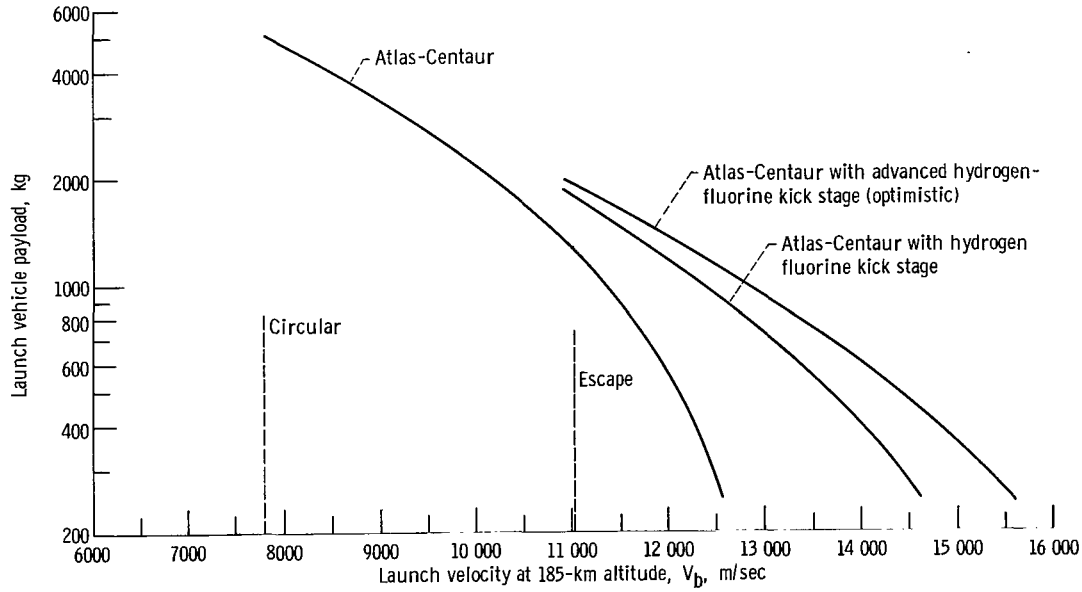

Figure 2. - Payload of Atlas-Centaur launch vehicles for various injection velocities at 185-kilometer injection altitude.

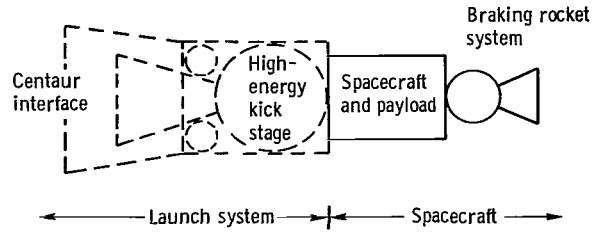

Total or initial mass of spacecraft at injection at Earth (from ACK curve)	M
Structure (including hardware contingency)	$M_{st} = 0.1\ M$
Chemical braking propellant at planet (capture missions)	M_p
Chemical braking propulsion hardware	$M_h = 0.2\ M_p$
Residual or gross payload	$M_\ell = M - M_{st} - M_p - M_h$
Braking propellant specific impulse, I_{sp}, sec	300

Figure 3. - Schematic and system summary for all-chemical-propulsion probe spacecraft.

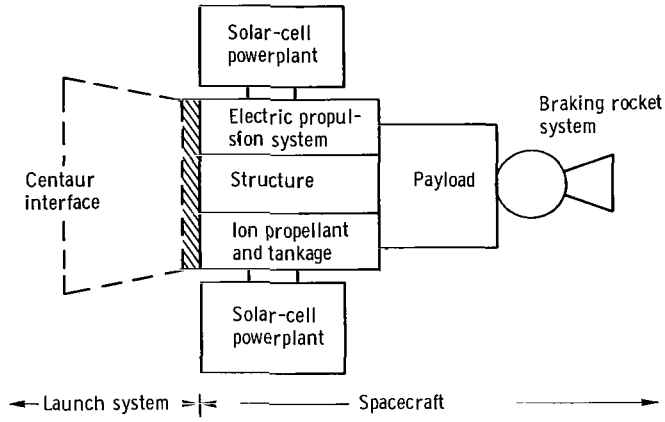

Total or initial mass of spacecraft at injection at Earth (from Atlas-Centaur curve)	M
Structure (including hardware contingency)	$M_{st} = 0.1\ M$
Powerplant, solar panels (50 lb/kW at Earth)	M_{pp}
Power regulation and ion thrusters (25 lb/kW at Earth)	M_c
Ion propellant, Mercury (depends on trajectory)	M_{pe}
Ion propellant tankage and hardware	$M_{he} = 0.1\ M_{pe}$
Chemical braking propellant at planet (capture missions)	M_p
Chemical braking propulsion hardware	$M_h = 0.2\ M_p$
Residual or gross payload	$M_\ell = M - M_{st} - M_{pp} - M_c - M_{pe} - M_{he} - M_p - M_h$
Braking propellant specific impulse, I_{sp}, sec	300

Figure 4. - Schematic and system summary for solar-electric-propulsion probe spacecraft. (Ion thruster efficiency given in fig. 5.)

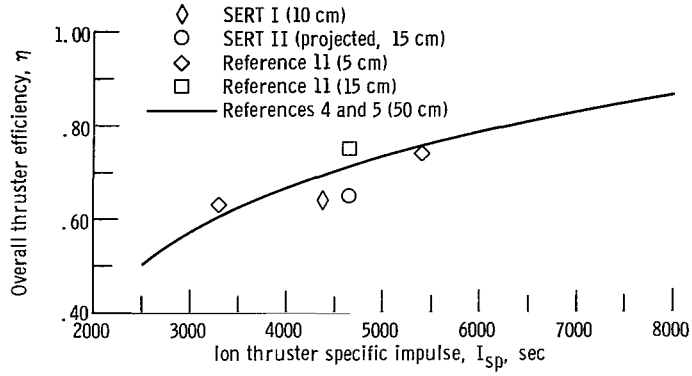

Figure 5. - Overall efficiency of electron bombardment mercury ion thruster.

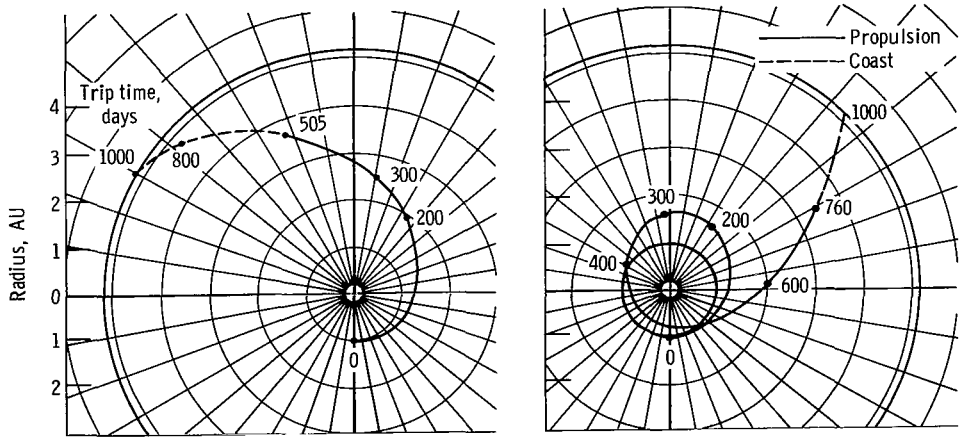

(a) Direct-transfer hyperbolic-electric (HE(A)), low-travel-angle case.

(b) 1.5-Revolution hyperbolic-electric (HE(B)), high-travel-angle case.

Figure 6. - Typical trajectory diagrams for direct-transfer and 1.5-revolution hyperbolic solar-electric-propulsion 1000-day Jupiter flyby missions.

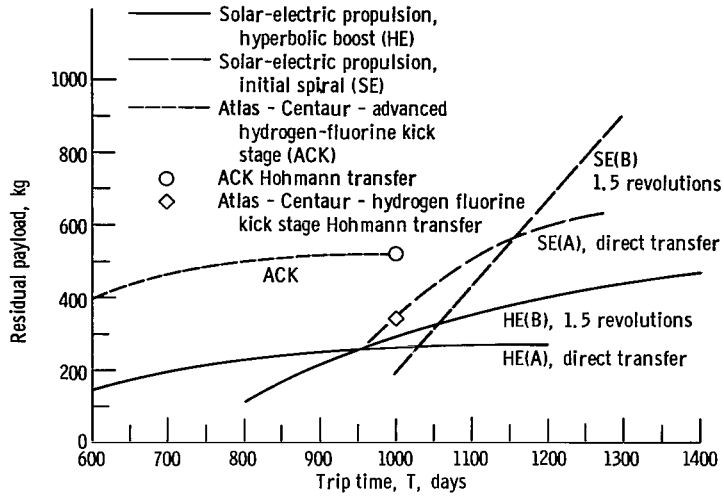

Figure 7. - Residual payload for Jupiter flyby missions with chemical and solar-electric propulsion.

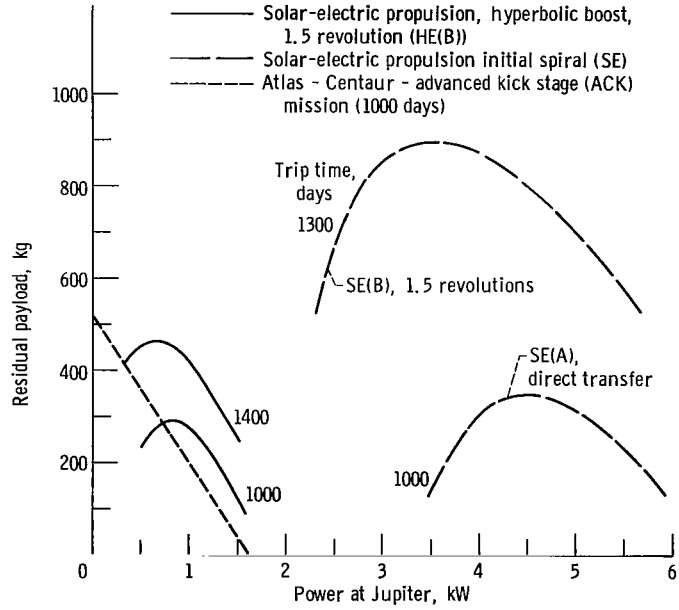

Figure 8. - Payload and power at planet for Jupiter flyby missions.

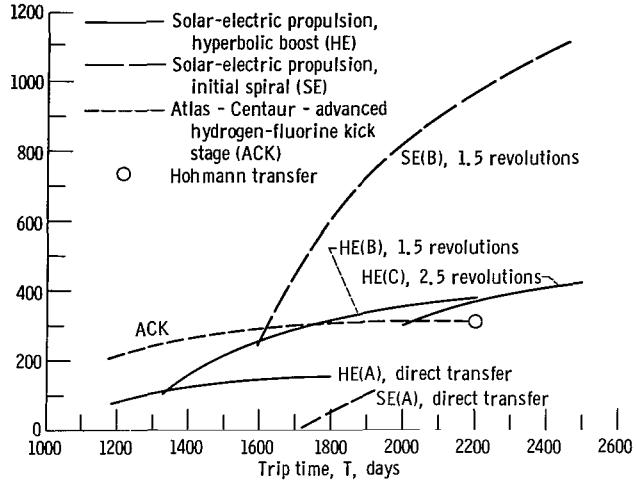

(a) Saturn.

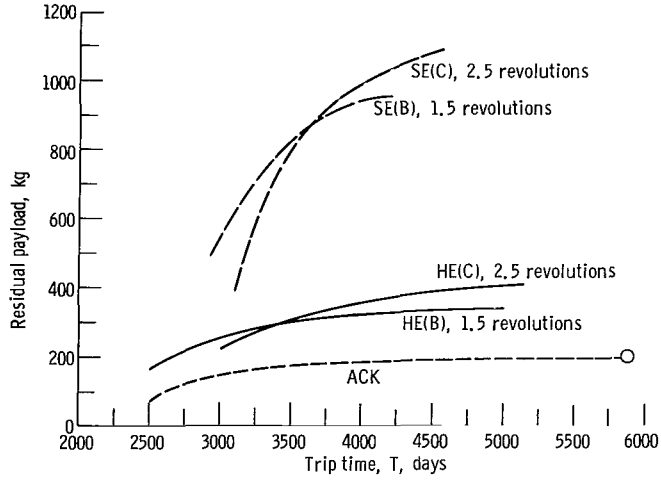

(b) Uranus.

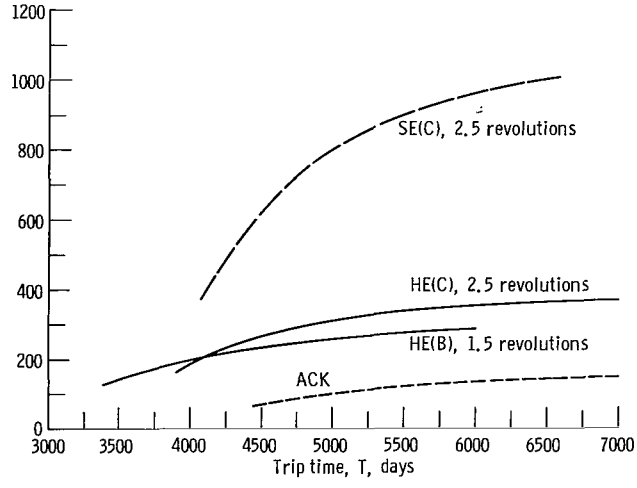

(c) Neptune.

Figure 9. - Residual payloads for flyby missions to planets beyond Jupiter with chemical propulsion and solar-electric propulsion.

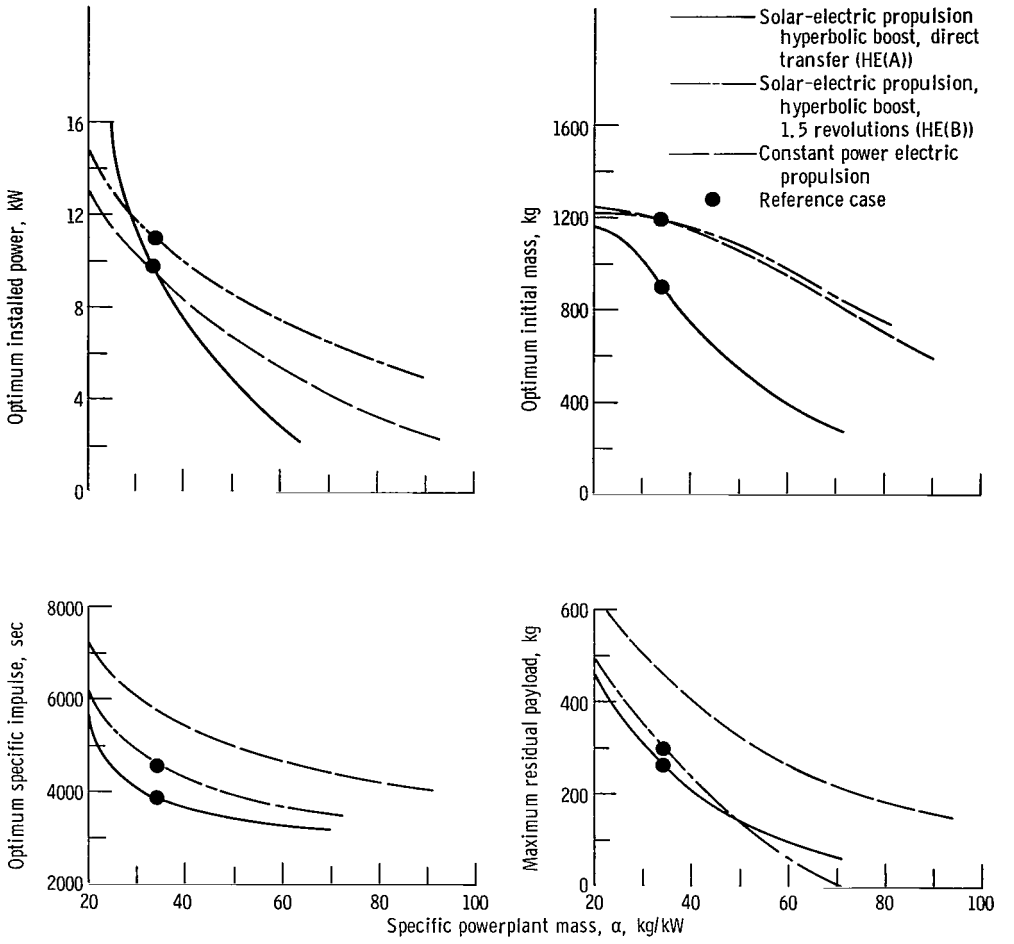

(a) Optimum installed power and specific impulse.

(b) Optimum spacecraft initial mass and maximum payload.

Figure 10. - Comparison of constant power and solar-electric propulsion for 1000-day Jupiter flyby.

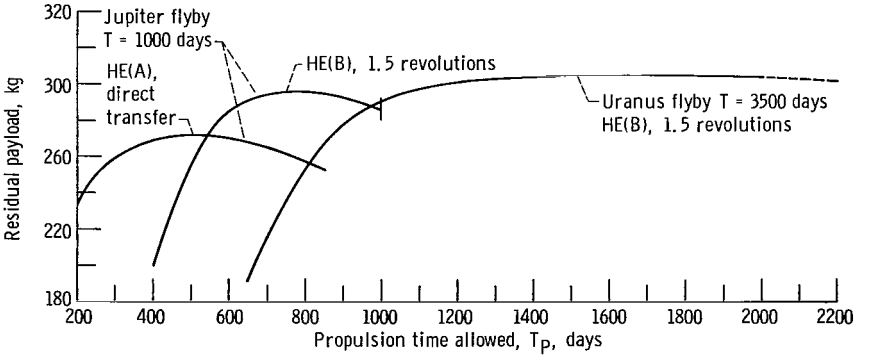

Figure 11. - Effect of allowed propulsion time on residual payload for Jupiter and Uranus flyby missions.

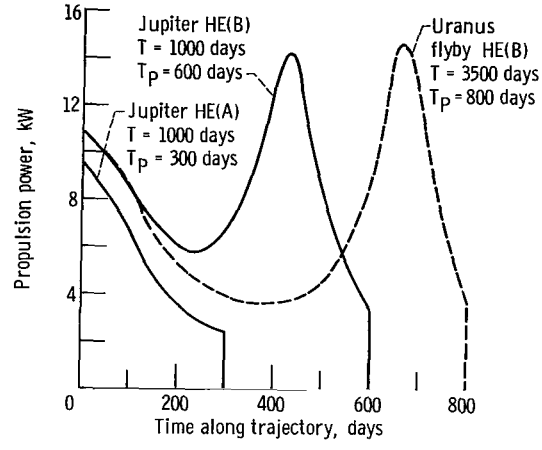

Figure 12. - Propulsion power history along Jupiter and Uranus flyby trajectories.

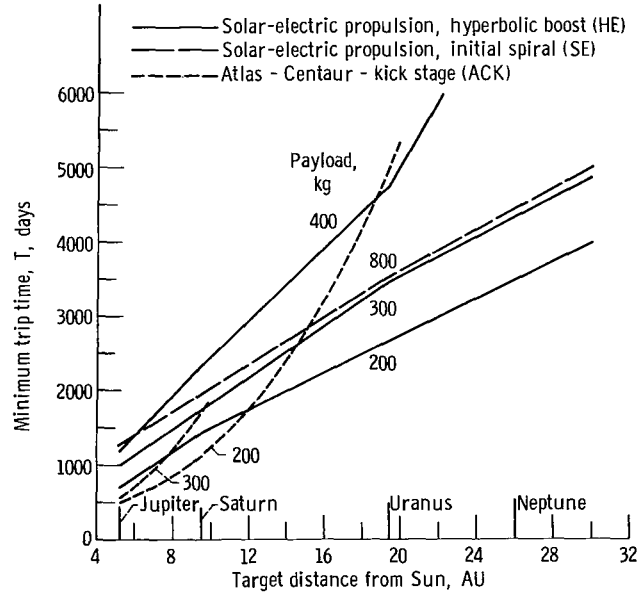

Figure 13. - Summary of minimum trip times for fixed payloads with various flyby mission profile types.

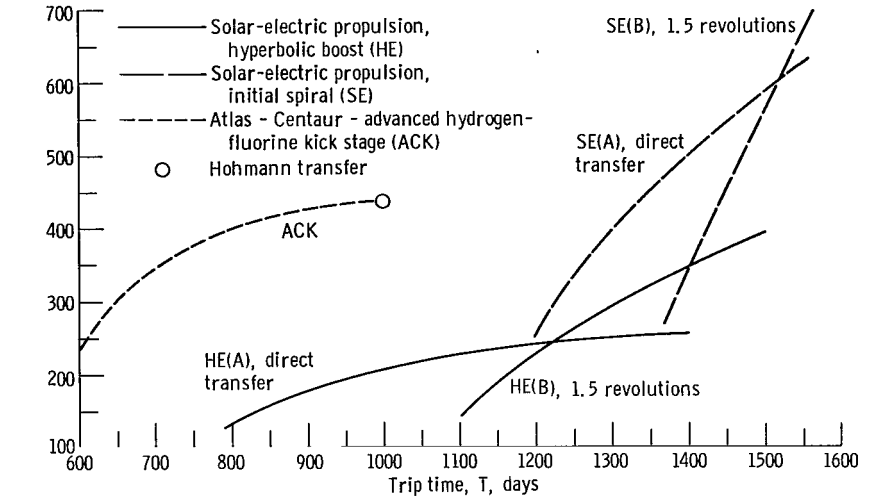

(a) Jupiter.

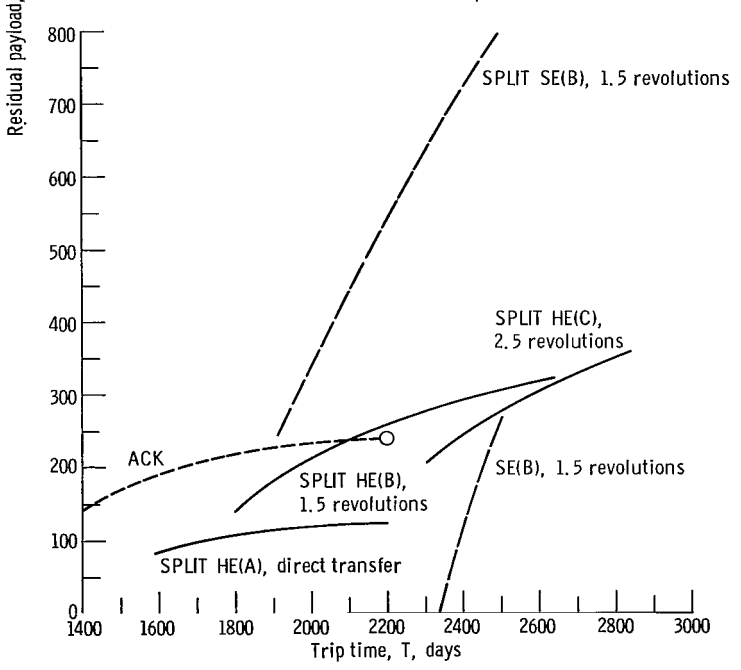

(b) Saturn.

Figure 14. - Residual payloads for capture missions with chemical and solar-electric propulsion. Loose elliptic final orbit.

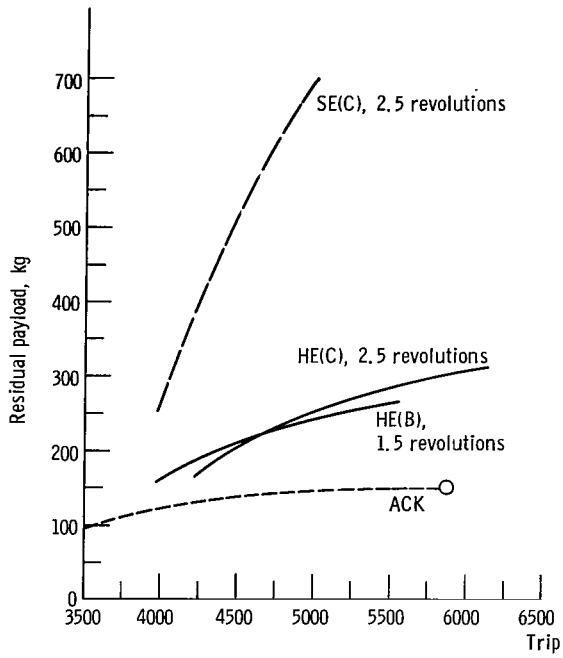

(c) Uranus, SPLIT.

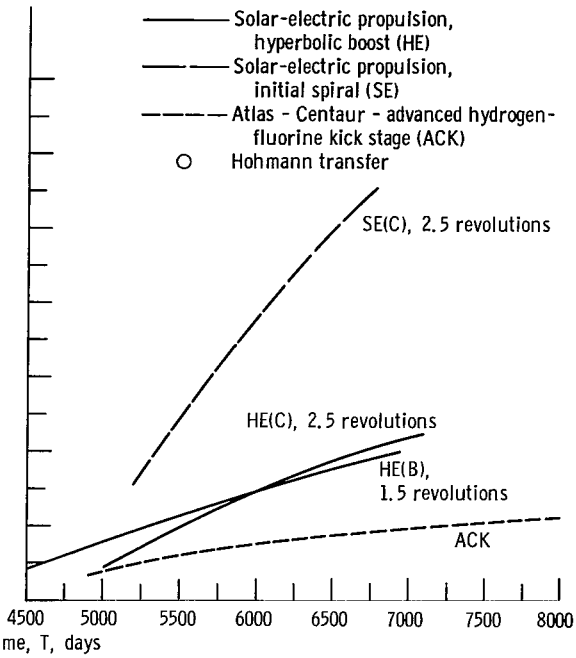

(d) Neptune, SPLIT.

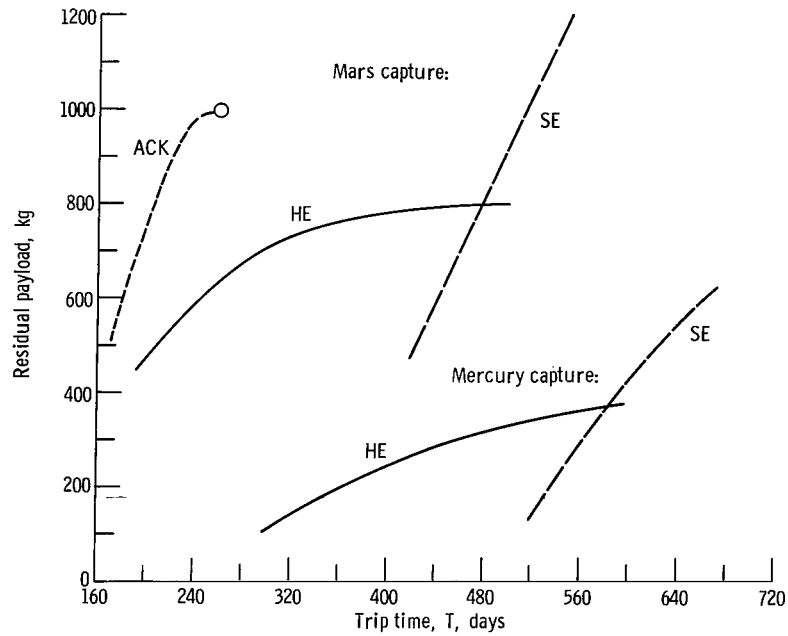

(e) Mars and Mercury. (ACK Mercury capture mission is not possible.)

Figure 14. - Concluded.

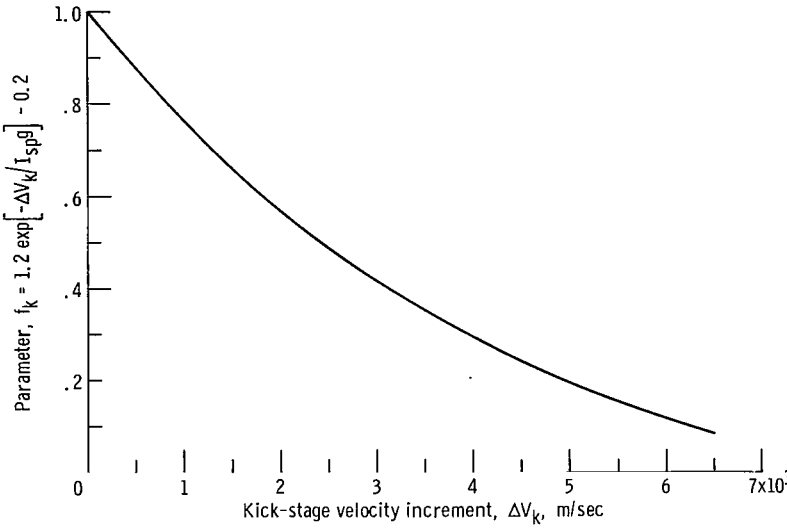

Figure 15. - Performance parameter for kick stage. Specific impulse, 460 seconds; ratio of hardware mass to propellant mass, 0.20.

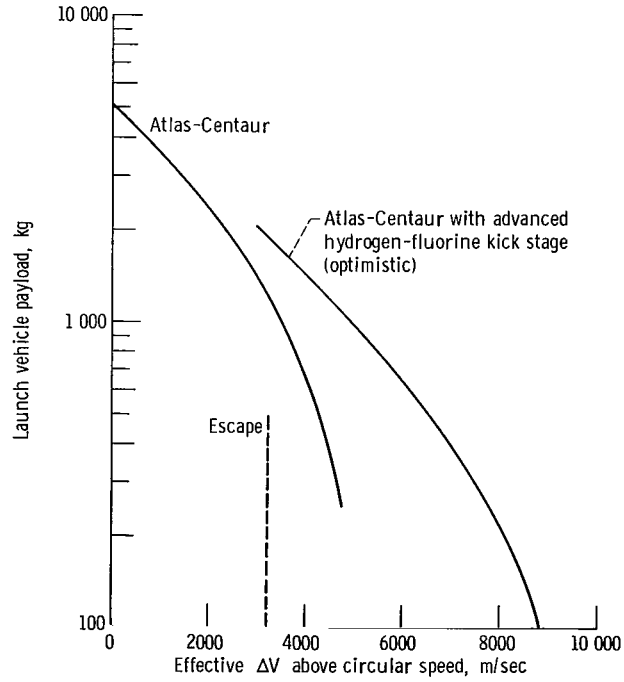

Figure 16. - Launch performance of Atlas-Centaur with optimized hydrogen-fluorine upper stage. Altitude, 185 kilometers; circular speed, 7800 meters per second.

NATIONAL AERONAUTICS AND SPACE ADMINISTRATION
WASHINGTON, D.C. 20546

OFFICIAL BUSINESS

FIRST CLASS MAIL

POSTAGE AND FEES PAID
NATIONAL AERONAUTICS AN
SPACE ADMINISTRATION

POSTMASTER: If Undeliverable (Section 158 Postal Manual) Do Not Retur

"The aeronautical and space activities of the United States shall be conducted so as to contribute . . . to the expansion of human knowledge of phenomena in the atmosphere and space. The Administration shall provide for the widest practicable and appropriate dissemination of information concerning its activities and the results thereof."

—NATIONAL AERONAUTICS AND SPACE ACT OF 1958

NASA SCIENTIFIC AND TECHNICAL PUBLICATIONS

TECHNICAL REPORTS: Scientific and technical information considered important, complete, and a lasting contribution to existing knowledge.

TECHNICAL NOTES: Information less broad in scope but nevertheless of importance as a contribution to existing knowledge.

TECHNICAL MEMORANDUMS: Information receiving limited distribution because of preliminary data, security classification, or other reasons.

CONTRACTOR REPORTS: Scientific and technical information generated under a NASA contract or grant and considered an important contribution to existing knowledge.

TECHNICAL TRANSLATIONS: Information published in a foreign language considered to merit NASA distribution in English.

SPECIAL PUBLICATIONS: Information derived from or of value to NASA activities. Publications include conference proceedings, monographs, data compilations, handbooks, sourcebooks, and special bibliographies.

TECHNOLOGY UTILIZATION PUBLICATIONS: Information on technology used by NASA that may be of particular interest in commercial and other non-aerospace applications. Publications include Tech Briefs, Technology Utilization Reports and Notes, and Technology Surveys.

Details on the availability of these publications may be obtained from:

SCIENTIFIC AND TECHNICAL INFORMATION DIVISION

NATIONAL AERONAUTICS AND SPACE ADMINISTRATION

Washington, D.C. 20546